Study of precipitation in martensitic Fe-C-Cr alloys during tempering: Experiments and modelling

Ziyong Hou

Licentiate Thesis

Stockholm 2015

Unit of Structures
Department of Materials Science and Engineering
School of Industrial Engineering and Management
Royal Institute of Technology
SE-100 44 Stockholm
Sweden

Akademisk avhandling som med tillstånd av Kungliga Tekniska Högskolan i Stockholm, framlägges för offentlig granskning för avläggande av Teknologie Licentiatexamen, fredagen den 4 december, kl. 13.00 i Kuben (N111), Brinellvägen 23, Materialvetenskap, Kungliga Tekniska Högskolan, Stockholm

---

ISBN 978-91-7595-756-2

Ziyong Hou **Study of precipitation in martensitic Fe-C-Cr alloys during tempering: Experiments and modelling**

Unit of Structures

Department of Materials Science and Engineering

School of Industrial Engineering and Management

Royal Institute of Technology

SE-100 44 Stockholm

Sweden

ISBN 978-91-7595-756-2

献给我的家人

To my beloved family

Abstract

Understanding the precipitation reaction is very important since precipitation hardening is one of the most effective strengthening mechanisms in metallic alloys. In martensitic steels, a tempering heat treatment is often performed. During tempering various new phases are precipitated and the spatial and temporal evolution of these precipitates strongly influences the properties of the steel, such as strength/ductility, creep, fatigue and hot corrosion resistance. Therefore, the possibility of quantitative modelling of the precipitation process will provide many opportunities for advanced materials and process design and optimization as well as service life assessments. The Fe-C-Cr system forms the basis for tool steels and is consequently used in many applications such as *e.g.* metal forming operations. They are characterized by a high hardness and good toughness, even at elevated temperatures.

In the present work, the as-quenched martensitic microstructures of four Fe-C-Cr alloys with varying Cr and C contents were characterized by Light Optical Microscopy (LOM) and Electron Microscopy. The effects of Cr and C on the morphology of martensite were investigated. It was found that Cr addition had a similar effect as C on the martensitic morphology and on the ratio of high-angle grain boundary (HAGB) to low-angle grain boundary (LAGB). However, the micro-hardness was unaffected by the Cr addition whilst it was strongly influenced by the C addition.

In addition, a quantitative experimental characterization of the precipitates formed during tempering of the martensite was performed. The Langer-Schwartz theory combined with the Kampmann-Wagner-Numerical (KWN) method, as implemented in the software TC-PRISMA, was used to predict the precipitation of carbides after tempering in one of the model alloys: Fe-0.15C-4.0Cr (mass%). The microstructure characterization of the as-quenched material provided vital input parameters for the modelling work and a comparison was made between the modelling predictions and the experimental results. The effect of parameters such as dislocation density, grain size and interfacial energy on the precipitation of carbides was discussed.

Keywords Fe-C-Cr alloy; Microstructure; Precipitates; Tempering of martensite; Electron microscopy; Modelling.

Sammanfattning

En god förståelse för utskiljningsreaktioner är mycket viktigt eftersom utskiljningshärdning är en av de mest effektiva härdningsmekanismerna i metallegeringar. För martensitiska stål utförs ofta en värmebehandling kallad anlöpning. Under anlöpningen skiljs nya faser ut och storleken och den rumsliga fördelningen av dessa utskiljningar påverkar starkt stålets egenskaper, såsom hållfasthet, seghet, krypmotstånd, utmattning och varmkorrosions-beständighet. Kvantitativ modellering av utskiljningsreaktioner skulle möjliggöra avancerad design av material och processer samt livslängdbedömningar.

Fe-C-Cr-systemet utgör grunden för verktygsstål och används i många tillämpningar såsom t.ex. metallformningsoperationer. De kännetecknas av en hög hårdhet och god seghet, även vid förhöjda temperaturer. I detta arbete har den martensitiska mikrostrukturen efter snabbkylning för fyra Fe-C-Cr-legeringar med varierande Cr-och C-halt undersökts med ljusoptisk mikroskopi (LOM) och elektronmikroskopi. Effekterna av Cr och C på morfologin hos martensit har studerats. Tillsatsen av Cr hade en liknande effekt som C på martensitens morfologi och på förhållandet mellan hög-vinkelkorngränser (HAGB) till låg-vinkelkorngränser (LAGB). Däremot var mikro-hårdheten opåverkad av Cr tillsats medan den tydligt påverkades av C-tillsats.

Dessutom har en kvantitativ experimentell karakterisering av de karbider som utskiljs under anlöpning av den martensitiska strukturen i Fe-0.15C-4.0 Cr (mass-%) genomförts. Modellering av karbidutskiljningen denna legering gjordes med programvaran TC-PRISMA, som bygger på teorin av Langer-Schwartz kombinerat med den numeriska metoden utvecklad av Kampmann-Wagner, och simuleringarna jämfördes med de experimentella resultaten. Den tidigare karakteriseringen av den martensitiska mikrostrukturen utgjorde en viktig del för modelleringsarbetet. Speciellt studerades effekten av parametrar såsom dislokationstäthet, kornstorlek och ytenergi på simuleringsresultaten.

Acknowledgements

First of all, I would like to give my thanks to my main supervisor, Joakim Odqvist and co- supervisor, Peter Hedström. Both of them have given me so much help during the past two years. Your kind help and great interest in my work is sincerely appreciated.

I would like to thank Dr. Qing Chen at Thermo-Calc Software AB for his helpful guidance to the TC-PRISMA software and for valuable discussions. Fredrik Lindberg and Niklas Pettersson at Swerea KIMAB are thanked for their guidance to the preparation of carbon replica samples and for help with the TEM. A special thanks goes to Henrik Jesperson (formerly with Uddeholms AB) and Maria Kvarnström at Uddeholms AB for their support with some of the TEM work.

I would like to acknowledge my colleagues in the Department of Materials Science and Engineering at KTH for providing a rigorous scientific research atmosphere. Especially, I would give to my thanks to all of whom gave me support and help: please forgive me since I cannot write down all of your names. Thanks to your company my life in Sweden has been far from dull and boring and I will never forget any of you.

This work was performed within the VINN Excellence Center Hero-m, financed by VINNOVA, the Swedish Governmental Agency for Innovation Systems, Swedish industry and KTH Royal Institute of Technology. Support from The China Scholarship Council (CSC), travel grants from Olle Erikssons Stiftelse för materialteknik and a research grant from the Swedish Steel Producers' Association are gratefully acknowledged.

Finally, I would like to express my greatest gratitude to my parents and my wife for their endless support.

Supplements

The present thesis is based on the following supplements:

Supplement 1

Microstructure of Martensite in Fe-C-Cr and its Implications for Modelling of Carbide Precipitation during Tempering

Ziyong Hou, Peter Hedström, Yunbo Xu, Di Wu and Joakim Odqvist

ISIJ International, 2014, 51(11): 2649-2656.

Supplement 2

Quantitative Modelling and Experimental Verification of Carbide Precipitation During Tempering of Martensite in an Fe-0.16 wt.%C- 4.0 wt.%Cr Alloy

Ziyong Hou, Peter Hedström, Qing Chen, Yunbo Xu, Di Wu and Joakim Odqvist

Submitted to Calphad.

The contributions by the author to the supplements of this thesis:

Supplement 1

Literature survey, sample preparation, experimental characterization, simulations, and writing of the first draft.

Supplement 2

Literature survey, sample preparation, experimental characterization, simulations, and writing of the first draft.

Contents

Chapter 1 Introduction

1.1 Background

Martensitic steels show an ultra-high strength and are widely used in applications such as *e.g.* metal forming operations and engineering machinery after their toughness have been improved by optimized heat treatments, such as tempering [1-3]. The tempering step is accompanied by precipitation of carbides which may result in increased strength and ductility if the dispersive particles are coherent with the matrix [4-11]. In the alternative scenario, several factors including migration of carbon atoms from the matrix phase, decomposition of retained austenite, precipitation and coarsening of the precipitates, recovery of dislocation structures and recrystallization, may lead to softening of the matrix phase [12-16]. Understanding of the precipitation reaction by advanced experimental and computational methodology is thus required for advanced material design and optimized heat treatments [2, 4, 17-21].

In the past decades, substantial research has been performed on characterizing the precipitation during tempering of steels [4, 6, 10, 11, 17, 21, 23-27] using various experimental methodologies such as *e.g.* the three-dimensional atom probe (3DAP) [28-29]. Both identification and quantification of the precipitates have been conducted, and several types of particles, such as MC, M_2C, M_3C, M_7C_3, $M_{23}C_6$ and M_6C may precipitate in iron based alloys [4, 10, 21-27]. The spatial and temporal evolution of these precipitates is determined by: the initial microstructure, influencing the interface type and nucleation sites, as well as the composition and tempering parameters, influencing the conditions at the phase interface in diffusional phase transformations [6, 11, 21, 23, 25-27]. Therefore, these factors are needed for an analysis of the precipitation in steels during tempering.

In addition to the experimental approach, several commercial software packages, for instance: PrecipiCalc, MatCalc, PanPrecipitation, MICRESS and DICTRA, have been used to simulate the precipitation process in different materials [30-39]. These software

packages have in many cases become important tools for material scientists in their daily research work. Recently, the software TC-PRISMA has been developed to simulate the co-precipitation of phases with concurrent processes of nucleation, growth and coarsening [40-43]. In many of the previous studies on precipitation during tempering of martensite the focus was on the qualitative or semi-quantitative evolution of the particle size distributions (PSD) over time but few studies have been performed on a quantitative basis. Thus, it is still a challenge to quantitatively model the precipitation in martensitic steels during tempering.

1.2 Objectives of the work

The aims of the present work are to quantitatively characterize and model the precipitation during tempering of a martensitic Fe-C-Cr steel. Specifically, the effect of the initial microstructure on the precipitation will be evaluated to increase the understanding of microstructure parameters such as dislocation density, grain size, *etc*. on the precipitation. Furthermore, the comparison between experimental data and simulations will provide a basis for further refinement of the modelling.

Chapter 2 Martensitic steels

2.1 Martensitic microstructure in steels

Martensite in steels may be regarded as a supersaturated solid solution of carbon atoms in the body-centered cubic (BCC) ferrite (α-Fe) phase or body-centered tetragonal (BCT) crystal structure [1, 12, 23, 44]. It is generated in a displacive and diffusionless transformation from austenite in case the cooling rate is above the critical cooling rate, sufficient to avoid all diffusional solid-state transformations such as the ferritic or pearlitic transformation [1, 44-46].

Martensite can have various morphologies, *e.g.* lath, butterfly, lenticular and thin plate, depending on several factors including chemical composition, transformation temperature, degree of supercooling, stacking fault energy and strength of austenite and martensite *etc.* [42, 44, 47-60]. In Fig.1, typical martensitic morphologies of Fe-C-Cr alloys are presented. The features of martensite such as mean size of lath/packet/block, austenite grain size and dislocation density *etc.* provide the initial information on *e.g.* nucleation sites for precipitation. Therefore, characterization of the initial microstructure is vital for understanding of the precipitation in martensite during tempering [5, 14, 42].

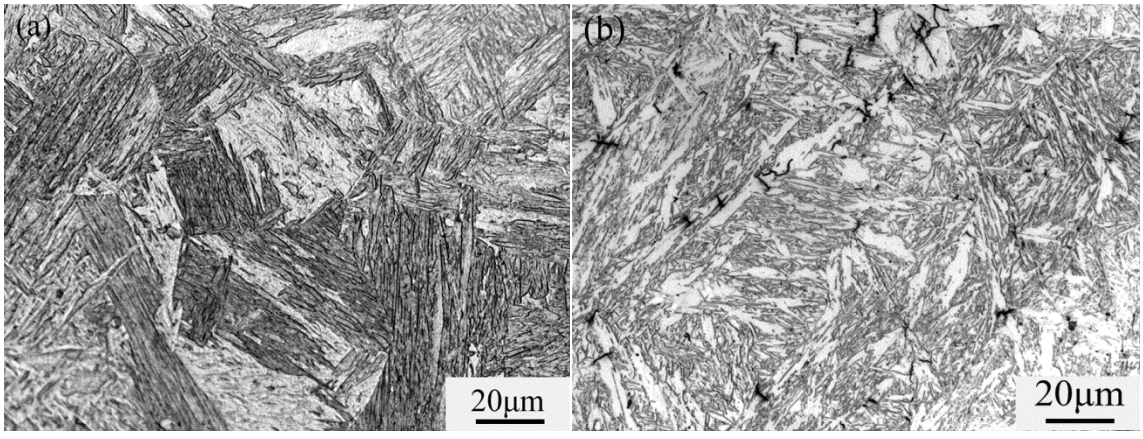

Fig.1 Typical martensite morphologies of Fe-C-Cr alloys (a) Fe-0.15C -1Cr (mass%), lath-shaped martensite, (b) Fe-1C-4Cr (mass%), plate-shaped martensite.

2.2 Tempering of martensite

The mechanical property of martensitic steels is usually modified with a heat treatment called tempering [1-3, 6, 15]. As a result, the toughness is improved due to the strain-stress release in martensite during tempering, and in certain cases the hardness can be increased by precipitation hardening. A good combination of toughness and strength is then achieved. In order to gain a good integrated performance extensive studies have been carried out on the tempering behavior of martensitic steels [7-9, 11, 21-26].

Tempering of martensitic steels is usually performed in the range between 150 and 700 ^{o}C [1]. The chemical composition and the required mechanical property for a certain alloy determine the selection of tempering temperature and time. The precipitates will nucleate at preferred nucleation sites, and the dislocation density decreases significantly during tempering. Meanwhile, the matrix phase changes during prolonged tempering, *e.g.* the martensite gradually transform from BCT structure to BCC structure due to that the carbon atoms leave the matrix to form carbide precipitates [12, 18, 23]. In Fig.2, SEM images of a tempered martensitic Fe-C-Cr alloy are presented. It is clearly seen that, after tempering at 700 ^{o}C for 1000 h the final microstructure consists of coarse particles in the ferritic matrix phase, while much finer particles and lath-shaped martensitic/ferritic structures are found at 500 ^{o}C.

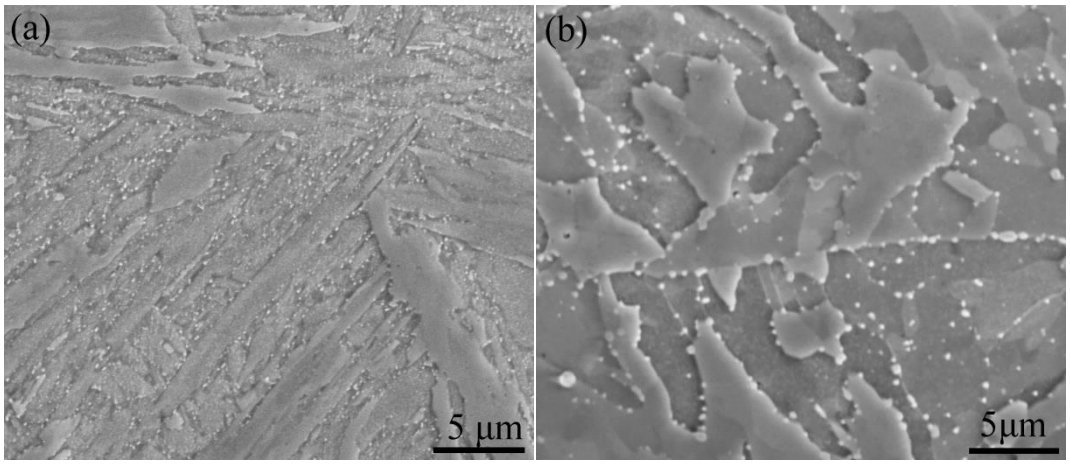

Fig.2 Microstructures of martensitic Fe-0.15C-4.0Cr alloy after tempering at 500 ^{o}C(a) and 700 ^{o}C (b) for 1000 h.

The precipitation reaction in martensitic steels during tempering has three stages, *i.e.* nucleation, growth and coarsening. The first step of precipitation is the nucleation where spatial fluctuations of phase structure and concentration develop within a supersaturated metastable alloy [9-10, 61]. From a modelling side, when a spherical embryo with a radius r^i is created by thermal fluctuation, the change of Gibbs free energy can be described by the following terms:

$$\Delta G = \frac{4}{3}\pi (r^i)^3 \Delta G_v + 4\pi (r^i)^2 \sigma + \frac{4}{3}\pi (r^i)^3 \Delta G_{st} \qquad \text{(Eq.2.1)}$$

where ΔG_v is the chemical free energy change per unit volume, σ is the specific interfacial energy and ΔG_{st} is the strain energy due to misfit between the nuclei and matrix. During growth of the nucleated precipitate the solubility of the alloying elements in the matrix will decrease towards the equilibrium composition. Later, as the equilibrium fraction of the second phases has precipitated, the coarsening of precipitates occurs, in which large particles grow and smaller particles dissolve [9, 10, 38, 40, 61]. Fig.3 shows TEM images of a Fe-0.15C-4.0Cr alloy after tempering at 700 ^{o}C for 0.5 h. It is clearly seen that the precipitates with different morphology form at lath boundaries as well as inside laths.

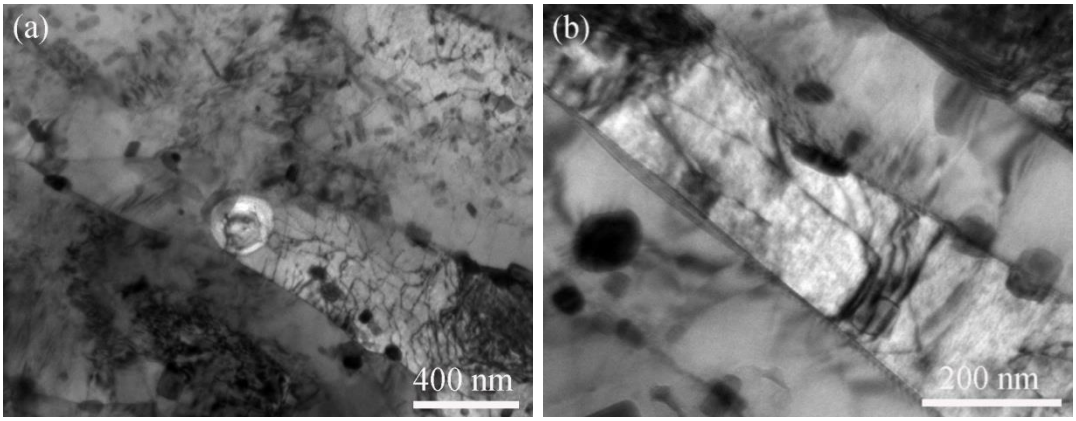

Fig.3 Precipitates on lath and dislocations (a) and on boundary (b) of a martensitic Fe-0.15C-4.0Cr alloy tempering at 700 ^{o}C for 0.5 h.

2.3 Precipitation hardening in martensitic steel

Precipitation hardening can be a potent strengthening mechanism in case the precipitation hardening overrides the softening of the martensite phase [4, 6, 9, 21]. This strengthening effect relies on the interaction between the dislocations and precipitates. In principle, two models have been used to describe the dislocation passage through a precipitate: cut through and Orowan looping, as seen in Fig.4 [8].

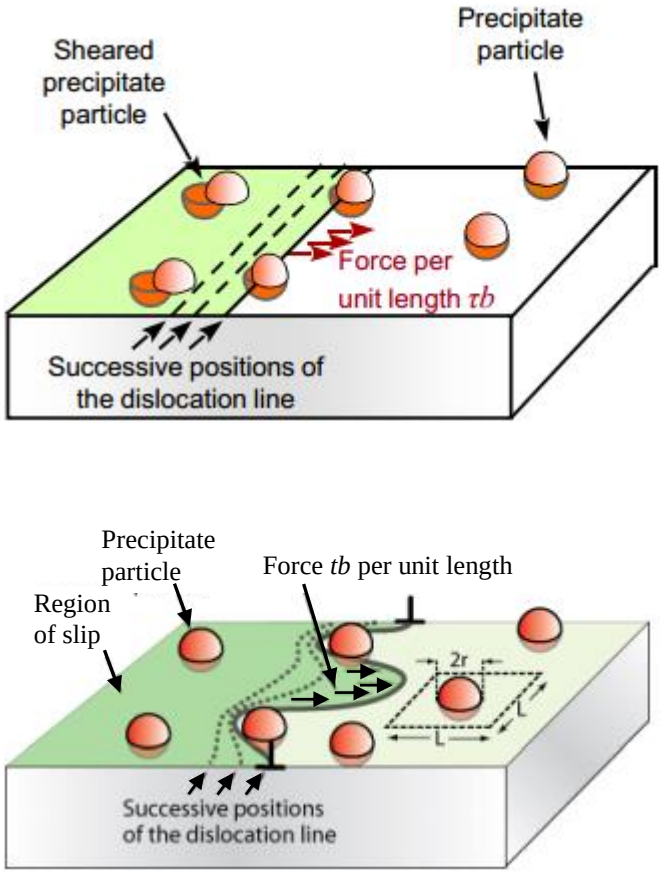

Fig.4 Interaction mechanism of precipitates and dislocations: (a) Cutting through precipitates; (b) Orowan looping, from Ref. [8].

Volume fraction, size (these two variables define the mean particle space in specific volume) and shape of particles *etc*. are vital parameters when considering the contribution of the precipitates to strengthening. The shear stress contributed, σ_p, by the precipitates can be expressed by [9]:

$$\sigma_P = \frac{\alpha G b}{L} \qquad \text{(Eq.2.2)}$$

where L is the mean space between the precipitates, G is the shear modulus of the iron matrix, b is Burger's vector, α is a dimensionless constant characterizing the obstacle mechanisms. The smaller the space L, the higher is the yield stress σ_P. This implies that quantitative characterization of the precipitates is needed to optimize the strength of materials.

Besides the impact on strength, the precipitates have many indirect effects. The precipitation of different intermetallic phases has been extensively studied in relation to material performance changes [62-67]. For instance, nanometer sized precipitates always plays a crucial role for the microstructure stability and resistance to creep and to hydrogen damage, even at elevated temperatures [65-67]. Thus, the ability to control the formation of precipitates, particularly in terms of size, distribution and fraction, provides a powerful tool in the optimization of the end properties of materials. Not only in the case of tempered martensite.

Chapter 3 Experimental methodology

In the present chapter the experimental methodologies, used for microstructure characterization and phase identification of precipitates in martensitic Fe-C-Cr steels, are presented. In Fig. 5, a schematic overview of the experimental procedures is presented.

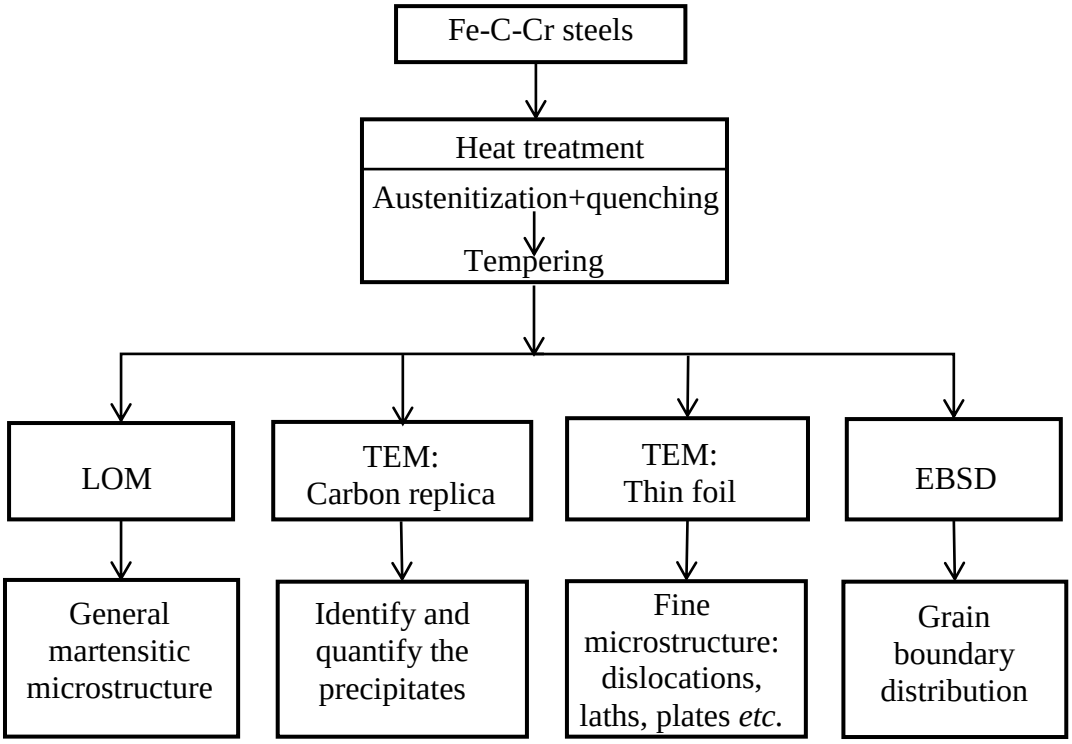

Fig.5 Schematic of the experimental procedures in the thesis.

3.1 Materials

Fe-C-Cr can be regarded as a basic system for tool steels. Four Fe-C-Cr steels with varying C and Cr content were selected as model alloys. In Table.1, the chemical compositions of the alloys used in the present work are listed. The phase diagrams of Fe-C-Cr alloys with fixed C and varying Cr from 0 to 5.0 mass% are shown in Fig.6, calculated by the Thermo-Calc software using the TCFE7 database [68, 69].

Table.1 Chemical compositions of the investigated alloys (in mass%)

No.	C	Cr	Si	Mn	S	Al	Cu	Ni
A	0.14	0.98	0.021	0.07	0.06	0.01	0.011	0.017
B	0.16	4.05	0.028	0.08	0.05	0.02	0.009	0.015
C	0.95	1.06	0.019	0.07	0.09	0.03	0.011	0.017
D	0.88	4.12	0.028	0.08	0.05	0.02	0.005	0.012

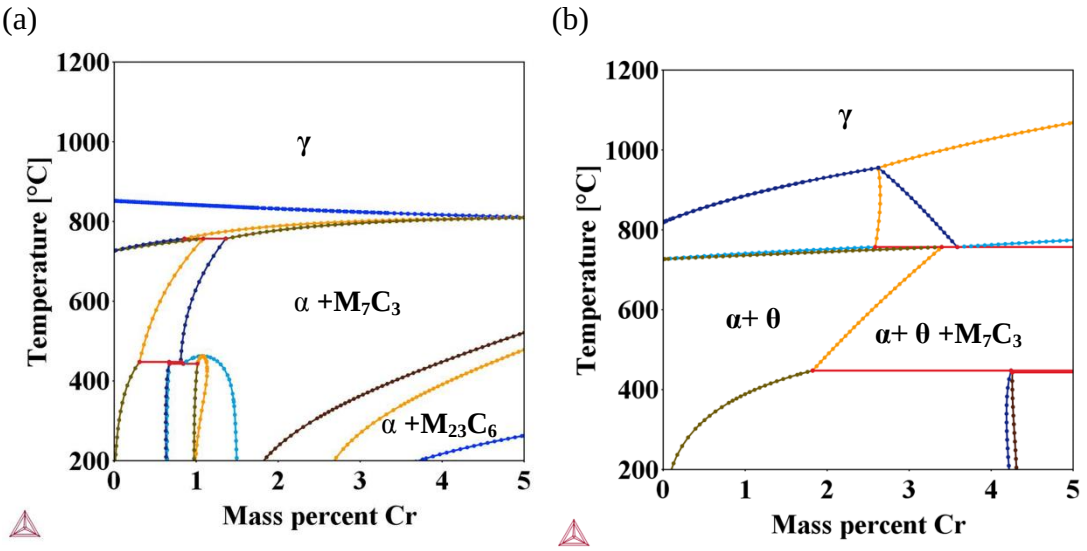

Fig.6 Phase diagram of Fe- C - Cr alloys with 0.15C (a) and 1.0C (mass%) (b), here, γ represents austenite; α represents ferrite, **θ** represents cementite.

3.2 Heat treatment

3.2.1 Austenitization and quenching

To achieve a martensitic microstructure, quenching from the austenitization temperature was performed. Small samples with dimensions $10 \times 10 \times 1$ mm^3, enabling a sufficiently high cooling rate in the whole sample, were cut from the hot-rolled plate, and austenitized at a temperature where the initial microstructure completely transform into austenite. According to the phase diagram shown in Fig.6, all the samples are fully austenitic at 1100^{o}C, and the austenitization was thus performed at that temperature for 10 min.

Prior to the heat treatments, calibration of the temperature for the Entech tube furnace was performed. The Entech tube furnace has a small isothermal heating zone of about 2 to 3 cm close to the center of the furnace. The samples were spot welded on the tip of a stainless steel rod and placed in the center of the furnace for austenitization in an Ar atmosphere. Subsequently, these austenitized samples were quenched in brine to room temperature [42].

3.2.2 Tempering

Tempering is usually applied after quenching to achieve the proper toughness, final hardness and dimensional stability [1]. Precipitation and spheroidization of the carbides accompanied by the recovery and recrystallization of matrix phase will occur in the martensite during tempering and it relates to the final properties of the material. Hence, the final properties of the steel can be controlled to some extent by controlling the tempering temperature and time. In order to understand the development of precipitation in martensitic Fe-C-Cr alloys during tempering, the as-quenched samples were tempered at 700 ^{o}C for times ranging from 5 s to 1000 h.

In the present study, three different methodologies were employed to try and eliminate the influence of heating time, oxidation and decarburization during the tempering. The details of the heat treatments are listed in Table.2.

Table.2 Experimental conditions and equipment used in the present study

Tempering time	5 s, 5min	30 min	5 h, 100 h, 1000 h
Methods	Sn-Bi metal bath	Tube furnace in Ar atmosphere	Vacuum-sealed quartz tube in Muffle furnace

Calibration of the temperature for the metal bath furnace and the Muffle furnace was performed prior to the tempering treatments. In Fig.7, a schematic illustration of the heating zone with dimensions 100×100 mm^2 in the Muffle furnace is shown.

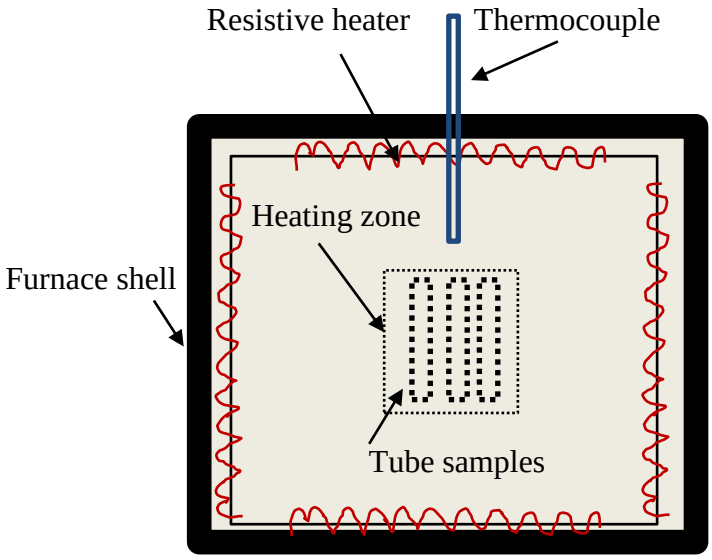

Fig.7 Schematic drawing of the Muffle furnace.

An example of a vacuum encapsulated sample in a quartz tube, aimed at long-term tempering (5 h, 100 h and 1000 h), is shown in Fig.8. A high-voltage spark tester was used to measure the vacuum before and after the heat treatments.

Fig.8 Vacuum-sealed sample prepared for long-term tempering.

3.3 Microstructure observations

3.3.1 Light optical microscopy (LOM)

To avoid heating of the quenched martensitic microstructure during hot mounting all as-quenched samples were cold mounted. The tempered samples were hot mounted before grinding and polishing. All the mounted samples were ground using $100^{\#}$ to $1500^{\#}$ SiC abrasive papers and polished using a 0.05 μm Al_2O_3 suspension. Then, these samples were etched by either 2% or 4% (vol.%) Nital, depending on the etching resistance of the alloys. The prepared samples were examined using a LEICA DMRM microscope.

3.3.2 Transmission electron microscope (TEM)

Electron microscopes, including transmission electron microscope (TEM) and scanning electron microscope (SEM), have a significantly higher resolution than LOM and are generally used to characterize the fine-scale microstructure in many materials. In steels, TEM is capable of imaging dislocations and twins, identifying crystallographic orientation relationships between adjacent grains, and identifying the crystal structures and lattice parameters of interesting phases, *etc.* Thin foil TEM samples are frequently used for TEM examinations [42, 43, 70]. Each sample was mechanically ground on SiC abrasive papers to 40 ~ 50 μm thickness and then small discs with diameters of 3 mm were punched out. These discs were subsequently electropolished using a Struers Tenupol-5 twin-jet electropolishing device. For the low carbon alloys (alloy A and alloy B), the prepared discs were electropolished using an electrolyte consisting of 9% perchloric acid and 91% ethanol (vol.-%) at a voltage of 20~30 V and -15 ~ -25^{o}C. For the high carbon alloys (alloy C and alloy D), the electrolyte was 5% perchloric acid, 15% glycerol, and 80% methanol (vol.-%), and the corresponding parameters were 20 ~ 30 V and 10 ~ 20 ^{o}C. The TEM experiments were performed on a JEOL JEM-2100F TEM operating at 200 kV.

3.3.3 Electron backscatter diffraction (EBSD)

A careful sample preparation process is required for successful EBSD analysis. Since artifacts can appear at each step of preparation, utmost care is necessary at all levels.

Special mechanical polishing was employed for the preparation of EBSD samples. A small load (15 N) was applied on the samples during grinding and polishing, aiming at reducing the imposed surface deformation. Finally, a 7 min polishing by 0.05 μm Al_2O_3 suspensions was performed, followed by a 30 s water-polishing. The prepared samples were investigated using a SEM LEO 1530 equipped with an EBSD detector. An acceleration voltage and step size of 20 kV and 0.2 μm, respectively, were used for the EBSD measurement in the present study.

3.4 Quantification of precipitates

3.4.1 Carbon extraction replica

In the past studies, characterization of precipitates in steels has been mainly carried out using TEM on thin foils and carbon extraction replicas. In comparison with the thin foil TEM samples, the carbon extraction replicas have several potential advantages: (1) distinct contrast between the precipitates and the matrix make semi-automatic (even automatic) measurement of the size distribution possible; (2) elimination of the influence of the matrix phase during chemical composition analysis; (3) large available area for TEM examination and statistical analysis; (4) avoiding a magnetic specimen that interacts with the electron beam. Thus, the carbon extraction replicas were prepared for quantitative analysis of the precipitates [43, 71].

A schematic of the carbon extraction replica sample preparation is shown in Fig.9. Firstly, the sample was carefully ground and polished as for metallographic samples. After that, the polished sample was chemically etched with a suitable etchant, in this case, 2 vol. % Nital for Fe-0.15C-4.0Cr steel after tempering at 700^{o}C. Thereafter, a carbon coating of 15 to 25 nm was deposited onto the etched surface using a Gatan 682 PECS™ (Precision Etching and Coating System, see in Fig.10). Then, the deposited carbon film was divided into several small squares (2×2 mm^2) by a sharp blade, and floated off in a solution of 10 vol.% perchlorate alcohol. A blend of distilled water and ethanol was applied to unfold the small carbon films after rinsing them in ethanol. Finally, several pieces of replicas were collected onto a copper grid and dried in ambient air.

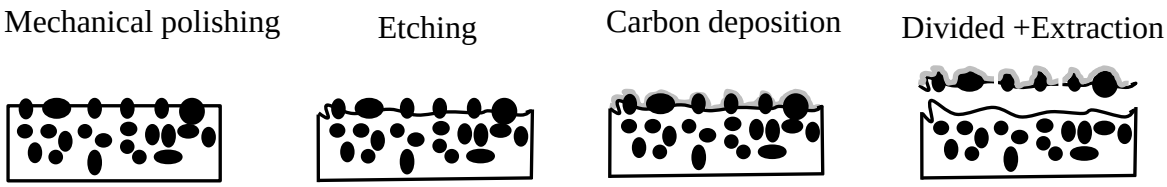

Fig.9 Schematic of carbon replica sample preparation.

Fig.10 Gatan 682 PECS™ for carbon coating.

3.4.2 Identification of precipitates

Selected area diffraction (SAD) patterns of the precipitate, in combination with its chemical composition analyzed by Energy-dispersive X-ray spectroscopy (EDXs), were used to identify the precipitates [72, 73]. Several similarly shaped particles were selected for each type of precipitate to ensure that the identification was correct. It was assumed that, one type of precipitate has a similar shape in a specific steel alloy. It was found that the faceted ones are M_7C_3 while elongated ones are $M_{23}C_6$ [42].

3.4.3 Mean radii of precipitates

After the identification of the precipitates the PSD analysis was also performed using multiple TEM bright field images taken from the carbon replicas. Automatic particle analysis was processed using the software ImageJ, and a considerable number of the precipitates were counted for each type of precipitate. First of all, an image threshold was

applied to the TEM image and then a binary image was created with black precipitates and white background. Thereafter, the area of each selected particle can be exported. Then, the data was categorized, representing each type of precipitates, based on the aspect ratio (see in Fig.11).

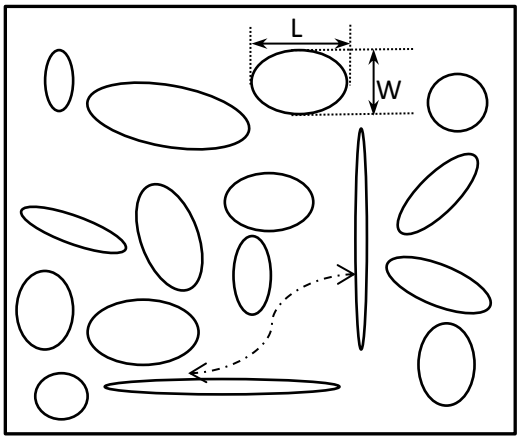

Fig.11 Different types of precipitates shown in different aspect ratio

The areas of the particles were converted to radii (assuming a spherical shape). The mean radius r_m of the precipitate *j* can be expressed by the total area A_j and number of particles counted (*n*):

$$r_m = \sqrt{\frac{1}{n}\sum\nolimits_{j=1}^{n} A_j \Big/ \pi} \qquad \text{(Eq. 3.1)}$$

Based on the number of particles in each class the PSD of each type of precipitate can be obtained.

3.4.4 Volume fraction of precipitates

In addition to the mean radius, the volume fraction is also a key factor in precipitation because both of them will determine the effect of the precipitates on the properties of the material, as mentioned earlier. Thus, quantitative analysis of the fraction of precipitates needs to be conducted. Chemical extraction is a relatively simple but effective method to separate the particles from the matrix. In the present case, 10 vol. % perchlorate ethanol was employed, and 100~210 mg of the sample was dissolved for each case in a glass

beaker. After filtering of the solution using a 15 nm pore size membrane filter, the residue was washed several times using methanol before drying it. Finally, the precipitate was weighed on a high precision digital electronic analytical balance scale (accuracy 0.01 mg). The mass fraction of each type of precipitate was determined, and subsequently, the volume fraction was calculated by considering the density of precipitate and matrix phase.

Chapter 4 Modelling of the precipitation

4.1 General information of the modelling

Many attempts have been made to modelling the precipitation in steels [10, 20, 22]. The Kampmann-Wagner numerical (KWN) model as implemented in the TC-PRISMA software can be used to predict precipitation reactions in multi-component and multiphase materials. The PSD, mean radii and number density of the precipitates during the whole tempering sequence can be calculated by solving a set of equations derived from certain assumptions for the nucleation and growth rates [40-42].

In the TC-PRISMA software, the nucleation, growth and coarsening of the precipitates are treated as concomitant processes. And, three growth models, *i.e.* simplified, advanced and binary dilute solution model, were implemented. For instance, the simplified growth model takes the operating tie-line across the bulk composition and avoids the computing of the tie-line iteratively from flux-balance equations during the tempering. Moreover, the growth model used in the present study, proposed by Chen, Jeppsson and Ågren (CJA) [39], takes both cross-diffusion terms and high supersaturations into account at the same time. Details about the model for nucleation, growth and coarsening used in the software can be found in Refs. [30, 39-41, 74].

4.2 Parameters for simulation

The thermodynamic and kinetic data needed for the simulation work are taken from the TCFE7 and MOBFE2 databases. Since input parameters, such as interfacial energy and dislocation density, have a strong influence on the simulation results, these parameters deserve special attention. When setting up a simulation a few candidate carbides are chosen, and the formed carbides during tempering are determined by TC-PRISMA. In a Fe-0.15C-4.0Cr alloy, the stable and metastable carbides at 700^{o}C are M_7C_3 and $M_{23}C_6$ respectively. This is in accordance with experimental results [42]. The interfacial energy, σ, depending on whether the particle is coherent, semi-coherent or incoherent with the matrix phase, is a key parameter in the precipitation modelling due to its cubic relation

with the nucleation and growth rates [39-42]. It can be estimated using an extension to Becker's model implemented in TC-PRISMA. Here, the σ of $M_{23}C_6$/BCC is calculated and kept as 0.272 Jm^{-2}, and that of M_7C_3/BCC is varied in a small range from 0.412 to 0.422 Jm^{-2}. Furthermore, the high density of dislocations are assumed to be the primary heterogeneous nucleation sites in the martensitic matrix during tempering. The dislocation density was varied in the range between 1.0×10^{14} and 1.8×10^{15} m^{-2}, depending on the microstructure and compositions [48]. The supersaturated martensite is treated as a BCC structure.

Chapter 5 Summary of key results

This chapter gives a summary of the key results in the present work, following the order: martensitic microstructure before tempering → precipitation in martensite during tempering → comparison between the experiments and the modelling results.

5.1 Martensitic microstructure before tempering

Since the initial microstructure, such as dislocation density, grain size, *etc*. is related to the subsequent precipitation of carbides during tempering, the quenched martensitic microstructures are presented. In Fig. 12, the inverse pole figures (IPF) from EBSD analysis of four Fe-C-Cr alloys are presented. A "classical" lath-like martensite as well as a prior austenite grain including several martensitic packets and blocks is clearly shown for 0.15%C alloys. With an increase in Cr from 1.0 to 4.0%, the lath units become much finer. On the other hand, a mixed microstructure of plate-like martensite and small portions of lath-like martensite are obtained in the Fe-1.0Cr-1.0C alloy. As the Cr content increases from 1.0 to 4.0 mass%, the aspect ratio of plate-like martensite increases. In addition, parts of the parallel units, resembling the packet structure of martensite in the low-carbon alloys, disappears. Cr plays a similar role to C on the martensitic morphology in Fe-C-Cr alloys.

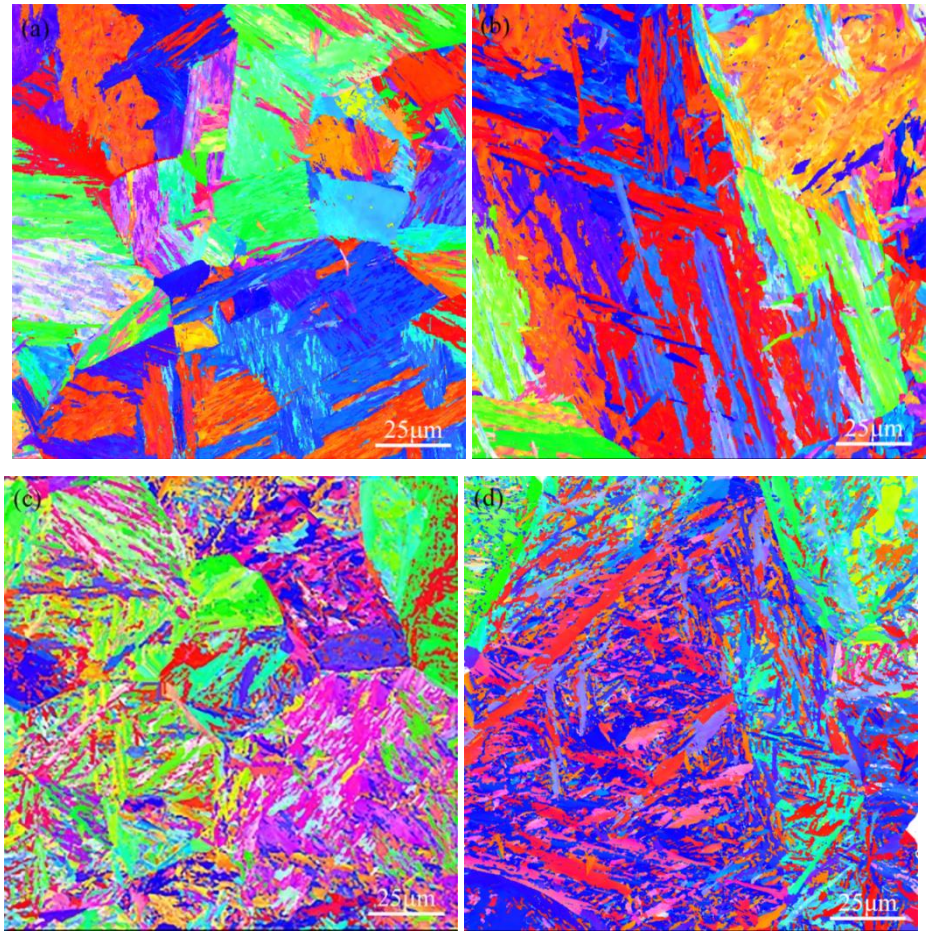

Fig.12 EBSD images for the four as-quenched Fe-C-Cr alloys, from Ref. [42].
(a) Fe-0.15C -1.0Cr; (b) Fe-0.15C -4.0Cr;
(c) Fe-1.0C -1.0Cr; (d) Fe-1.0C -4.0Cr.

Fig.13 shows the hardness of the present four Fe-C-Cr alloys, and data from the literature for Fe-C and Fe-C-X alloys were also plotted. The hardness increases with increasing C content but does not depend on other elements, such as Cr, Ni, significantly in steels. When the Cr content increases from 1.0 to 4.0% the micro-hardness of low-carbon steels changes slightly despite the significant changes of the martensitic morphology. The highest micro-hardness of the four Fe-C-Cr alloys was acquired in alloy C despite its lower Cr content compared to alloy D. This is ascribed to the slightly higher C content in alloy C as compared with alloy D. It can be concluded that the micro-hardness of Fe-C-Cr alloys is mainly dependent on C content while the martensitic morphology is related to both C and Cr content.

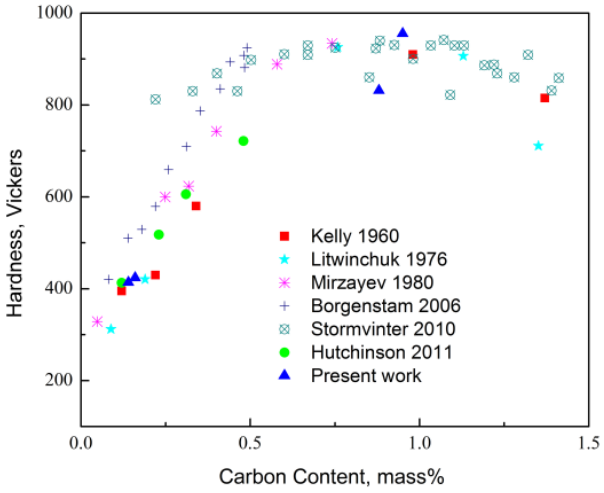

Fig.13 Hardness of the investigated alloys in comparison with literature data for Fe-C and Fe-C-X alloys, from Ref. [42].

5.2 Precipitation in martensite during tempering

Fig.14 shows TEM images of the precipitates in the Fe-0.15C-4.0Cr alloy tempered for different times at 700^{o}C. It can be seen that, the nucleation of precipitates has occurred after 5s. With the tempering proceeding, the precipitates grow and two types of precipitates, *i.e.* faceted and elongated, can be found after all tempering times. From SAD it can be concluded that faceted precipitates represent M_7C_3 and elongated precipitates correspond to $M_{23}C_6$.

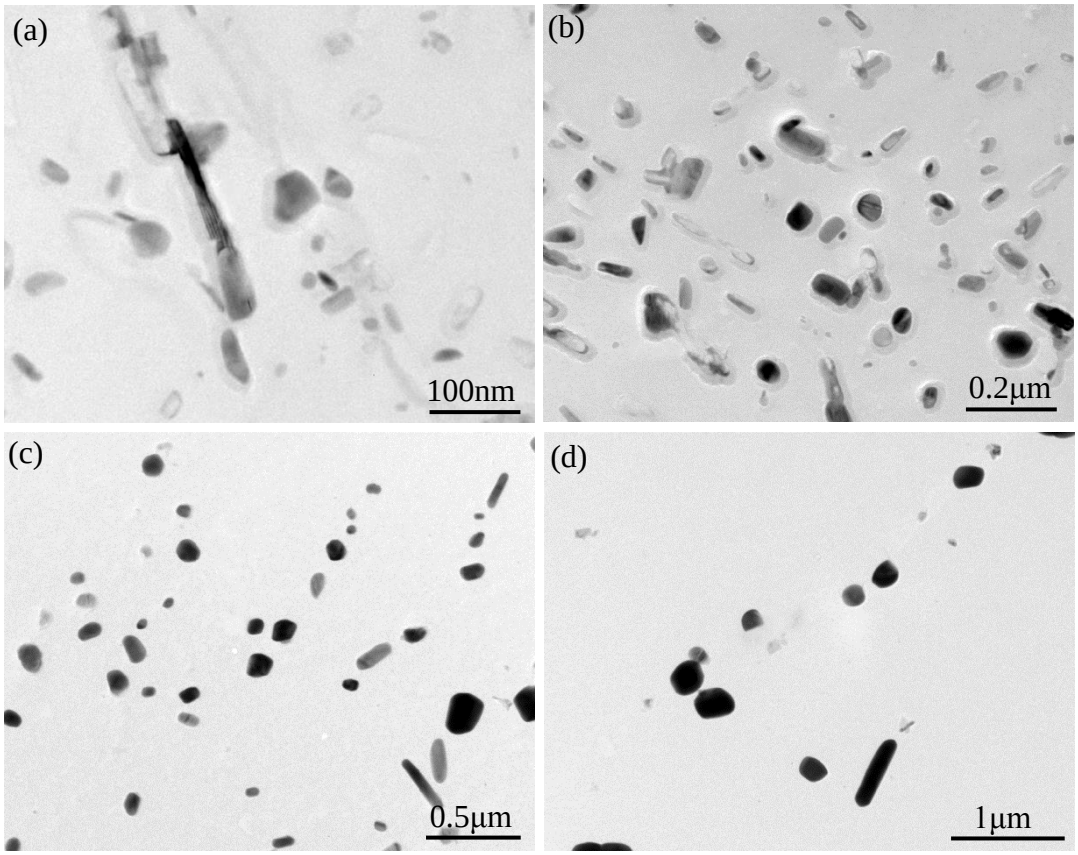

Fig.14 TEM micrograph of Fe-0.15C - 4.0Cr alloy tempered at 700°C for (a) 5 s; (b) 5 min; (c) 5 h; (d) 1000 h.

5.3 Comparison between modelling and experimental results

The counted precipitates of the samples tempered for different times are listed in Table. 3. More than 263 M_7C_3 carbides are considered. However, only a few $M_{23}C_6$ carbides have been found within an identical area as that counted for M_7C_3.

The mean radii of the precipitates from experimental work and calculated by TC-PRISMA are shown in Fig.15. The mean radii of both M_7C_3 and $M_{23}C_6$ are sensitive to the interfacial energy. It is also known that the mean radii are influenced by grain size, and dislocation density if assuming them as nucleation sites. In Fig.16, the difference between the volume fractions of precipitates calculated using TC-PRISMA and from extraction experiments is presented. From both the modelling and experimental results,

the volume fraction of M_7C_3 stays stable after the nucleation stage is completed, and metastable $M_{23}C_6$ disappears after long-term tempering.

Table.3 Mean radius and counting number of particles for different tempering times

Tempering time	5 s	5 min	30 min	5 h	100 h	1000 h
Mean radius of M_7C_3	16	21	26	56	131	134
Mean radius of $M_{23}C_6$	15	24	32	63	94	156
Number of counted M_7C_3	263	286	288	324	294	337
Number of counted $M_{23}C_6$	16	14	10	8	5	1

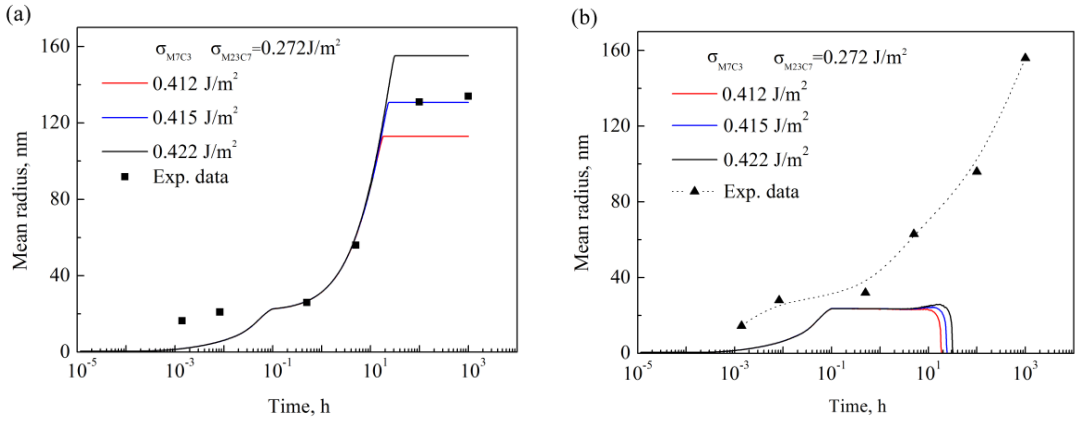

Fig.15 Mean radii of M_7C_3 (a) and $M_{23}C_6$ (b) of the alloy tempered for different times, obtained from TC-PRISMA (solid lines) and experiments (symbols).

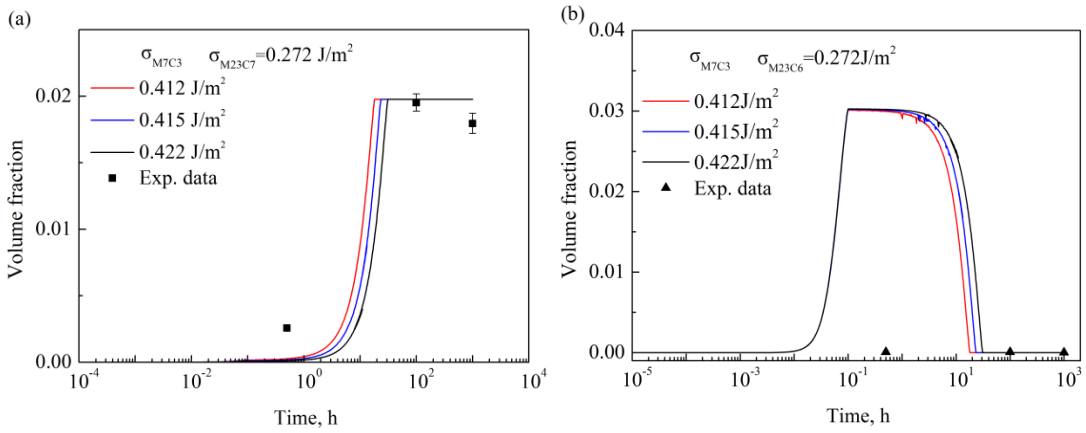

Fig.16 Volume fraction evolution of M_7C_3 (a) and $M_{23}C_6$ (b) during tempering simulated using TC-PRISMA (solid lines) and from extraction experiments (symbols).

For M_7C_3, the simplified growth model can capture the evolution of the precipitation during tempering expect for the early stage, see Figs. 15a and 16a. However, for $M_{23}C_6$, there is a huge difference between the simulation results and experimental measurements no matter how the input parameters are varied, see Figs. 15b and 16b.

Based on an analysis using the advanced growth model [43], the growth of M_7C_3 at the early stage shows a transition from the non-partitioning local equilibrium (NPLE) to partitioning local equilibrium (PLE) condition due to the size dependent capillarity effect [39]. This transition leads to a deviation of the modelling result for M_7C_3 compared to the experimental results at the beginning stage of precipitation. For PLE, distribution of substitutional elements is necessary, thus the transformation is slow; in NPLE condition, the transformation is controlled by the carbon diffusion and no substantial components redistribution occurs at the interface, so the transformation is extremely fast compared to that in PLE condition.

The $M_{23}C_6$ volume fraction is overestimated in the simulations, and a very low fraction of $M_{23}C_6$ can still be found experimentally after 1000 h of tempering. Several critical factors should be considered for this difference between the modelling and experiments. Since

$M_{23}C_6$ was reported to be nucleated at grain boundaries, less nucleation sites compared to the assumed dislocation density and high diffusivity along boundaries may be the cause of the large particles at various boundaries which do not dissolve even though they are predicted to do so from the modelling.

Chapter 6 Conclusions

In this work the as-quenched microstructures of four Fe-C-Cr alloys have been studied, followed by a study of the precipitation in a martensitic Fe-0.15C-4.0Cr alloy during tempering by means of experiments and modelling. The results are summarized as follows:

(1) The dominant martensitic microstructure is lath martensite in low carbon Fe-C-Cr alloys while a mixture of plate and lath martensite is obtained in high carbon Fe-C-Cr alloys.

(2) With an increased Cr content from 1.0 to 4.0 mass%, the martensitic microstructure becomes finer for low carbon steels, and high-angle boundaries are more frequent and planar defects can be found. Cr in Fe-C-Cr alloys has a similar effect as C on the martensitic morphology but only a slight influence on the hardness.

(3) Faceted M_7C_3 and elongated $M_{23}C_6$ are detected in a martensitic Fe-0.15C-4.0Cr alloy during tempering at 700^{o}C; both types of carbides are nucleated at various boundaries as well as within the lath, but most of the coarsened precipitates are found at boundaries.

(4) The interfacial energy as well as dislocation density has a significant influence on the precipitation as seen from the modelling.

(5) The simplified growth model using the tie-line across the bulk composition underestimate significantly the size of particles that grow under the NPLE condition, leading to a deviation of the modelling result for M_7C_3 compared to experimental results at the beginning stage of precipitation.

Chapter 7 Future Work

In order to fully understand and model the precipitation behavior in Fe-C-Cr alloys during tempering, a number of future challenges should be addressed:

(1) The dislocation density has a large influence on the precipitation when the dislocations are assumed to be the heterogeneous nucleation sites. However, since it is hard to get a precise value this parameter was taken from previous works for a similar microstructure and composition. The dislocation density could instead be measured using experimental methods such as TEM techniques, X-ray diffraction (XRD) and neutron techniques, and thus it could make the modelling results much more reliable and improve the predictive capability.

(2) In the present work, the effect of interfacial energy on the precipitation has been studied, and the modelling result shows that the interfacial energy is a critical parameter for the precipitation. However, reliable experimental data of the interfacial energy is still limited due to the difficulty of measuring the solid/solid interfacial energy. The interfacial energy in the present work was estimated using the nearest neighbour broken bond (NNBB) approach and adjusted slightly to fit the experimental data. The orientation relationship between the matrix and the precipitate has not been considered though it is known that the orientation relationship is a crucial factor when calculating the interfacial energy. Therefore, better estimates of the interfacial energy could be made by establishing the orientation relationship between the precipitate and matrix.

(3) In the present work the precipitates are nucleated at various boundaries and in martensite laths. The condition for each type of nucleation site, *e.g.* interfacial energy is probably quite different. However, in the present work, such details about the nucleation sites are not considered. The fraction of each nucleation site type for each precipitate phase could be quantified and used to improve the modelling.

(4) As already described, the shortest tempering time is from 5s at 700^{o}C, at which the nucleation stage seems to be already completed. Since the very early stage and the chemical composition of the precipitate has a strong influence on later growth and coarsening, an analysis of short-time tempered samples by advanced experimental methods *e.g.* Atom-probe tomography (APT), may shed some light on what is the

governing condition at the carbide/matrix phase interface: NPLE, PLE or something else.

References

[1] H.K.D.H. Bhadeshia, R. Honeycombe: Steels: microstructure and properties. The tempering of martensite steels (Oxford, OX: United Kingdom Elsevier Publishing Company, 2006), 183-208.

[2] G.E. Totten: Steel heat treatment: Metallurgy and technologies (London, LON: LLC Taylor & Francis Group, 2006), p207.

[3] V. Velay, G. Bernhart, L. Penazzi: Cyclic behavior modeling of a tempered martensitic hot work tool steel, Int. J. Plasticity, 2006, 22 (3): 459-496.

[4] J. Andersson: Secondary hardening in some low-chromium hot-work tool steels. Ph.D thesis. Chalmers University of Technology. 2011.

[5] S. M. H. Hoseiny: Influence of microstructure on the machinability of prehardened mould steels. Chalmers University of Technology. 2011.

[6] F. Abe, M. Taneike1, K. Sawada: Alloy design of creep resistant 9Cr steel using a dispersion of nano-sized carbonitrides, Int. J. Pres. Ves. Pip, 2007, 84 (1-2): 3-12.

[7] M.C. Mataya, R.A. Fournelle: Fatigue behavior of a nial precipitation hardening medium carbon steel, Metall. Trans. A, 1978, 9 (7): 917-925.

[8] M.F. Ashby, H. Shercliff, D. Cebon: Materials: Engineering, Science, Processing and Design, Published by Elsevier, L td. Butterworth-Heinemann. 2007, 209.

[9] J.W. Martin: Precipitation hardening. Butterworth-Heinemann, Oxford. 1968.

[10] S. Yamasaki: Modelling precipitation of carbides in martensitic Steels. Ph.D thesis, Darwin College, University of Cambridge. 2004.

[11] P. Michaud, D. Deslagnes, P. Lamesle, M. H. Mathon, C. Levaillant: The effect of the addition of alloying elements on carbide precipitation and mechanical properties in 5% chromium martensitic steels, Acta Mater., 2007, 55 (14): 4877-4889.

[12] T.Ohmura, K.Tsuzaki, S.Matsuoka: Evaluation of the matrix strength of Fe-0.4 wt% C tempered martensite using nanoindentation techniques. Philos. Mag. A, 2002, 82(10): 1903-1910.

[13] T.Ohmura, T.Hara, K.Tsuzaki: Evaluation of temper softening behavior of Fe-C binary martensitic steels by nanoindentation. Scr. Mater., 2003, 49(12):1157-1162.

[14] T.Ohmura, T.Hara, K.Tsuzaki: Relationship between nanohardness and microstructures in high-purity Fe-C as-quenched and quench-tempered martensite. J. Mater. Res., 2003, 18(6):1465-1470.

[15] T.Ohmura, K.Tsuzaki: Evaluation of matrix strength of Fe-C as-quenched and quench-tempered martensite using nanoindentation techniques. J. Phys. IV France, 2003, 112: 267-270.

[16] T. Ohmura, T. Hara, K. Tsuzaki, H. Nakatsu, Y. Tamura: Mechanical characterization of secondary-hardening martensitic steel using nanoindentation. J. Mater. Res., 2004, 19(1): 79-84.

[17] C.E.I.C. Ohlund, Erik Schlangen, S. Erik Offerman: The kinetics of softening and microstructure evolution of martensite in Fe-C-Mn steel during tempering at 300 ℃. Mater. Sci. Eng. A 2013, 560: 351-357.

[18] N. Mébarki: Relationship between microstructure and mechanical properties of tempered martensitic steel. Ph.D. thesis, Ecole Nationale Supérieure des Mines Paris (in French). 2003.

[19] M.A. Asadabad, S. Kheirandish, A.J. Novinrooz: Microstructural and mechanical behavior of 4.5Cr-2W-0.25V-0.1C steel, Mater. Sci. Eng. A, 2010, 527 (6): 1612-1616.

[20] K. Frisk: Simulation of precipitation of secondary carbides in hot work tool steels, Mater. Sci. Tech., 2012, 28 (3): 288-294.

[21] A.M. Sherman, G.T. Eldis, M. Cohen: The aging and tempering of iron-nickel-carbon martensites, Metall Trans, A, 1983, 14: 995-1005.

[22] H.J. Jou, P. Voorhees, G.B. Olson: Computer simulations for the prediction of microstructure/property variation in aero turbine disks, Proc. Superalloys 2004, Champion, PA, USA, September 2004, TMS, 877-886.

[23] L. Cheng, C.M. Brakman, B.M. Korevaar, E.J. Mittemeijer: The tempering of iron-carbon martensite; dilatometric and calorimetric analysis, Metall. Trans, A. 1988, 19 (10): 2415-2426.

[24] J. Janovec, M. Svoboda, A. Vyrostkova, A. Kroupa: Time-temperature-precipitation diagrams of carbide evolution in low alloy steels, Mater. Sci. Eng. A, 2005, 402 (1-2): 288-293.

[25] K. Miyata, M. Igarashi, Y. Sawaragi: Effect of trace elements on creep properties of. 0.06C-2.25Cr-1.6W-0.1Mo-0.25V-0.05Nb steel, ISIJ Int., 1999, 39 (9): 947-954.

[26] K. Frisk: Simulation of precipitation of secondary carbides in hot work tool steels, Mater. Sci. Technol., 2012, 28 (3): 288-294.

[27] X.B. Hu, M. Zhang, X.C. Wu and L. Li: Simulations of coarsening behavior for $M_{23}C_6$ carbides in AISI H13 steel, J. Mater. Sci. Technol., 2006, 22 (2): 153-158.

[28] D.N. Seidman: Three-Dimensional Atom-Probe Tomography: Advances and Applications, Annu. Rev. Mater. Res. 2007. 37:127-158.

[29] D.N. Seidman, K. Stiller: An atom-probe tomography primer, MRS Bull., 2009. 34: 717-724.

[30] M. Perez, A. Deschamps: Microscopic modelling of simultaneous two phase precipitation: application to carbide precipitation in low carbon steels, Mater. Sci. Eng. A, 2003, 360 (1-2): 214-219.

[31] P.F. Shi, A. Engström, B. Sundman, J. Ågren: Thermodynamic calculations and kinetic simulations of some advanced materials, Mater. Sci. Forum, 2011, 675-677: 961-974.

[32] A. Costa e Silva, L. Nakamura, F. Rizzo: Application of computational modeling to the kinetics of precipitation of aluminum nitride in steels, J. Min. Metall. B, 2012, 48 (3): 471-476.

[33] R. Mukherjee, T.A. Abinandanan, M.P. Gururajan: Phase field study of precipitate growth: Effect of misfit strain and interface curvature, Acta Mater., 2009, 57 (13): 3947-3954.

[34] L.Q. Chen: Phase-field models for microstructure evolution, Annu. Rev. Mater. Res., 2002, 32: 113-140.

[35] A. Borgenstam, A. Engström, L. Höglund, J. Ågren: A tool for simulation of diffusional transformations in alloys, J. Phase Equilib., 2000, 21: 269-280.

[36] W. Cao, S.L. Chen, F. Zhang, K. Wu, Y. Yang, Y.A. Chang, R. Schmid-Fetzer, W.A. Oates: PANDAT software with PanEngine, PanOptimizer and PanPrecipitation for multi-component phase diagram calculation and materials property simulation, Calphad, 2009, 33(2):328-342.

[37] N. Fujita: Modelling carbide precipitation in alloy steels. Ph.D thesis, University of Cambrige, 2000.

[38] P. Schaaf, A. Krämer, S. Wiesen, U. Gonser: Mössbauer study of iron carbides: mixed carbides M_7C_3 and $M_{23}C_6$, Acta Metal. Mater., 1994, 42 (9): 3077-3081.

[39] Q. Chen, J. Jeppsson, J. Ågren: Analytical treatment of diffusion during precipitate growth in multicomponent systems, Acta Mater., 2008, 56 (8): 1890-1896.

[40] O. Prat, J. García, D. Rojas, J.P. Sanhueza, C. Camurri: Study of nucleation, growth and coarsening of precipitates in a novel 9%Cr heat resistant steel: Experimental and modeling, Mater. Chem. Phys., 2014, 143 (2): 754-764.

[41] O. Prat, J. García, D. Rojas, C. Carrasco, G. Inden: Investigations on the growth kinetics of laves phase precipitates in 12% Cr creep-resistant steels: experimental and DICTRA calculations, Acta Mater., 2010, 58 (18): 6142-6153.

[42] Z.Y. Hou, P. Hedström, Y.B. Xu, D. Wu, J. Odqvist: Microstructure of martensite in Fe-C-Cr and its implications for modelling of carbide precipitation during tempering, ISIJ Int., 2014, 54 (11): 2649-2656.

[43] Z.Y. Hou, P. Hedström, Q. Chen, Y.B. Xu, W. Di, J. Odqvist: In manuscript 2015.

[44] L. Delaey: Diffusionless transformations. In: Cahn R W, Haasen P, Kramer E J (eds.) Materials Science and Technology, Vol. 5, Phase Transformations in Materials. 1991, VCH, Weinheim, Germany.

[45] V. A. Pozdnyakov: Mechanisms of martensite nucleation at grain boundaries, Dokl. Phys., 2007, 52 (1): 24-28.

[46] B.C. Muddle, J.F. Nie: Martensite. encyclopedia of materials: science and technology, Elsevier Science Ltd. 2001, p5189-p5193.

[47] G. Kruss, A.R. Marder: The morphology of martensite in iron alloys, Metall. Trans. 1971, 2:2343-2357.

[48] S. Morito, J. Niskawa, T. Maki: Dislocation density within lath martensite in Fe-C and Fe-Ni alloys, ISIJ Int., 2003, 43 (9): 1475-1477.

[49] S. Morito, H. Tanaka, R. Konishi, T. Furuhara, T. Maki: The morphology and crystallography of lath martensite in Fe-C alloys, Acta Mater., 2003, 51 (6): 1789-1799.

[50] T. Maki: Microstructure and mechanical behavior of ferrous martensite, Mater. Sci. Forum, 1990, 56-58: 157-168.

[51] M. Umemoto, K. Minoda, I. Tamura: Some characteristics of the substructure of lenticular martensite in Fe-Ni-C alloys, Metallography, 1982, 15 (2): 177-191.

[52] P. M. Kelly, J. Nutting: The martensite transformation in carbon steels, Proc. Roy. Soc. London A, 1960, 259: 45-48.

[53] P.M. Kelly: The martensite transformation in steels with low stacking fault energy, Acta Metall., 1965, 13 (6): 635-646.

[54] M. Umemoto, E.Yoshitake, I. Tamura: The morphology of martensite in Fe-C, Fe-Ni-C and Fe-C-Cr alloys, J. Mater. Sci., 1983, 18 (10): 2893-2904.

[55] A. Stormvinter, P. Hedström, A. Borgenstam: Transmission electron microscopy study of plate martensite formation in high-carbon low alloy steels, J. Mater. Sci. Technol., 2013, 29 (4): 373-379.

[56] S. Morito, H. Tanaka, R. Konishi, T. Furuhara, T. Maki: The morphology and crystallography of lath martensite in Fe-C alloys, Acta Mater., 2003, 51 (6): 1789-1799.

[57] T. Furuhara, S. Morito, T. Maki: Morphology, substructure and crystallography of lath martensite in Fe-C alloys, J. Phys. IV France, 2003, 112 (1): 255-258.

[58] A. Stormvinter, P. Hedström, A. Borgenstam: Investigation of lath and plate martensite in a carbon steel, Solid State Phenomena, 2011, 172-174: 61-66.

[59] S. Morito, X. Huang, T. Furuhara, T. Maki, N. Hansen: The morphology and crystallography of lath martensite in alloy steels, Acta Mater., 2006, 54 (13): 5323-5331.

[60] S. Morito, Y. Adachi, T. Ohba: Morphology and crystallography of sub-blocks in ultra-low carbon lath martensite steel, Mater. Trans., 2009, 50 (8): 1919-1923.

[61] R. Kampmann, R. Wagner Softening: Kinetics of precipitation in metastable binary alloys-theory and application to Cu-1.9 at % Ti and Ni-14 at % Al, in decoposition of Alloys: the Early stages, P. Haasen,V. Gerold, R.Wagner and M.F. Ashby, eds., Pergamon Press, Oxford. 1984.

[62] H. Zurob, C. Hutchinson, Y. Bréchet, G. Purdy: Modeling recrystallization of microalloyed austenite: effect of coupling recovery, precipitation and recrystallization, Acta Mater., 2002, 50 (12): 3077-3094.

[63] T. Gladman: The Physical Metallurgy of Microalloyed Steels, The Institute of Materials, London, 2002.

[64] M. Hillert: Inhibition of grain-growth by 2nd-phase particles, Acta Metall., 1988, 36 (12): 3177-3181.

[65] T. Yokota, T. Shiraga: Evaluation of hydrogen content trapped by vanadium precipitates in a steel, ISIJ Int. 2003, 43 (4): 534-538.

[66] K. Maruyama, K. Sawada, J. Koike: Strengthening mechanisms of creep resistant tempered martensitic steel, ISIJ Int., 2001, 41 (6): 641-653.

[67] F. Abe: Bainitic and martensitic creep-resistant Steels, Curr. Opin. Solid State Mater. Sci., 2004, 8: 305-311.

[68] J.O. Andersson, T. Helander, L. Höglund, P.F. Shi, B. Sundman: Thermo-Calc and DICTRA, Computational tools for materials science. Calphad, 2002, 26: 273-312.

[69] Thermo-Calc Software TCFE7 Steels/Fe-alloys database version 7, (Accessed 15 June 2015).

[70] D. V. Sridhara Rao, K. Muraleedharan, C. J. Humphreys, TEM specimen preparation techniques, Microscopy: Science, Technology, Applications and Education A. Méndez-Vilas and J. Díaz (Eds.) 2010, 1232-1244.

[71] M.J. Jr. Donachie, O.H. Kriege: Phase extraction and analysis in super alloys-summary of investigation by ASTM committee E-4 task group 1, J. Mater., 1972, 7: 269-278.

[72] K.L. Lin: Phase identification using series of selected area diffraction patterns and energy dispersive spectrometry within TEM, Microsc. Res., 2014, 2: 57-66.

[73] A. L. Rivas, E. Vidal, D.K. Matlock, J.G. Speer: Electrochemical extraction of microalloy carbides in Nb-steel. Revista de Metalurgia, 2008, 44 (5): 447-456.

[74] D. Kashchiev, Nucleation: Basic Theory with Applications, Butterworth Heinemann, Oxford, 2000.